TELKOMNIKA Indonesian Journal of Electrical Engineering
Vol.12, No.6, June 2014, pp. 4250 ~ 4257
DOI: 10.11591/telkomnika.v12i6.4268

Magnetic Resonance Imaging Fusion by 3D Compactly Supported Shearlet Transform

Chang Duan*[1,2], Qihong Huang[3], Shuai Wang[1], Xuegang Wang[1], Hong Wang[1]
[1]School of Electronic Engineering, University of Electronic Science and Technology (UESTC)
[2]Research Institute of Electronic Science and Technology, UESTC
[3]Electronic Engineering College, Chengdu University of Information Technology (CUIT)
*Corresponding author, e-mail: pertinnax@163.com

Abstract

T2 and quantitative susceptibility mapping (QSM) of* magnetic resonance imaging *(MRI) images provide different type inner structure information of scanned organs. If they can be properly fused into one set, the details of the scaned organ can be revealed more clearly. In this paper, a 3D MRI image fusion method based on 3D compactly supported shearlet transform (3D-CSST) and 3D dual tree compactly supported shearlet transform (3D-DT-CSST), is proposed, which can overcome the limitation, loss of inter layer correlative information, of conventional 2D image fusion methods. 3D-DT-CSST is our modification of 3D-CSST, which is approximate shift invariant. It can improve the performance of fusion method. The proposed method is evaluated by 4 groups of MRI images of human brains. The results suggest that the proposed method has a better performance than conventional 2D wavelet, 2D DT-CWT and 3D wavelet, 3D DT-CWT based fusion methods, and 3D-DT-CSST based method is better than 3D-CSST based method.*

Keywords*: medical image fusion, compactly supported shearlet transform, quantitative susceptibility mapping*

1. Introduction

Medical image fusion is a special case of image fusion, and has been studied for decades. It has widely applied in medical diagnosis [1, 2]. It refers to extract and merge the feasible information from different source images, which were captured by different kinds of devices, such as CT, MRI, PET etc., or different configurations of the same device, such as MRI T2* and quantitative susceptibility mapping (QSM). Special devices or special configurations of the same device reveal different aspect of scanned organs. The information of source images is correlated or, more likely, complementary. For instance, CT images provide the details of dense hard tissues, MRI images provide the inner structure of soft tissues: T2* provide the contrast of the tissue relaxation time, QSM provide susceptibility contrast information, such as caused by a range of endogenous magnetic biomarkers and contrast agents e.g. iron, calcium and gadolinium (Gd). If different data can be properly fused, the fused data contains all the sailent information of the scanned organ, which can reveal the details of inner structure more clearly than each single source. Previously, all source data need to be registered. 3D T2* magnitude images and QSM images are getting from the same scan, and therefore, have already exactly registered.

Currently many researches on medical fusion method only consider the 2D case. While many diagnostic devices can provide 3D images, and the value of each voxel in the 3D images is correlated not only to the adjacent points in same layer, but also to the points in neighboring layers. Therefore, it's necessary to develop the 3D image fusion method instead of 2D image fusion method which cause the loss of the consistency in the third dimension.

Fusion methods can be performed in spatial domain or certain transformed domain. In spatial domain, the intuitive fused image is selected as the weighted average image of source images [3]. This kind of methods is relatively easy to implement, but its performance is low and always cause the decrease or even loss of some feasible information. The transformed domain based fusion methods are usually following the steps: 1) performing the forward transform to sources images, 2) acquiring the fused coefficients from coefficients of source images under

Received August 30, 2013; Revised December 21, 2013; Accepted January 24, 2014

fusion rules, 3) performing backward transform to fused coefficients to get the fused image. In this type of methods, the research works usually focused on two points: the choice of the transform and the design of fusion rule.

Many multi scale transforms are applied in fusion methods, such as DWT [4], lifting wavelet [5], complex wavelet [6], curvelet [7], shearlet [8], etc. Shearlets emerged in recent years among the most successful frameworks for the efficient representation of multidimensional data. Indeed, many transforms are introduced to overcome the limitation of traditional multi-scale transforms of poor ability of capturing edges and other anisotropic features. However, shearlet transform stands out since it has many advantages uniquely: a single or finite set of generating functions; optimally sparse representations for multi-dimensional data; a unified treatment of the continuum and digital realms; and a compactly supported transform etc. With so many advantages above, shearlet transform has been widely utilized into many image processing tasks such as de-noising [9], edge detection [10], enhancement [11], etc. In this paper, the conventional 3D Compactly Supported Shearlet Transform (3D-CSST) is improved to overcome its lacking of shift invariance property, through the Dual Tree (DT) structure, and then both 3D-CSST and 3D-DT-CSST are selected as the transforms for the 3D medical image fusion.

Three fusion rules are utilized in this paper: maximum points' modulus (MPM), which considers only the value of single point; maximum regional energy (MRE), which considers the information for local region [12], and treats each points of the region equally and maximum sum of modified laplacian [13], which also considers the information in local region, but treats the center point of the region and the points around it differently. These three classic fusion rules are expanded into 3 dimensions. In order to evaluate the performance of proposed method, the quality indices also are expanded into 3 dimensions.

The rest of the paper is organized as followings. In section 2, the implementation of 3D-CSST and the modification of 3D-DT-CSST are introduced. In section 3, fusion method based on 3D-CSST and 3D-DT-CSST with three fusion rules is proposed. From the experiments of section 4, the comparison of 2D and 3D methods and the performance about the proposed methods are illustrated and discussed. Finally, we draw conclusions in section 5.

2. 3D Compactly Supported Shearlet Transform

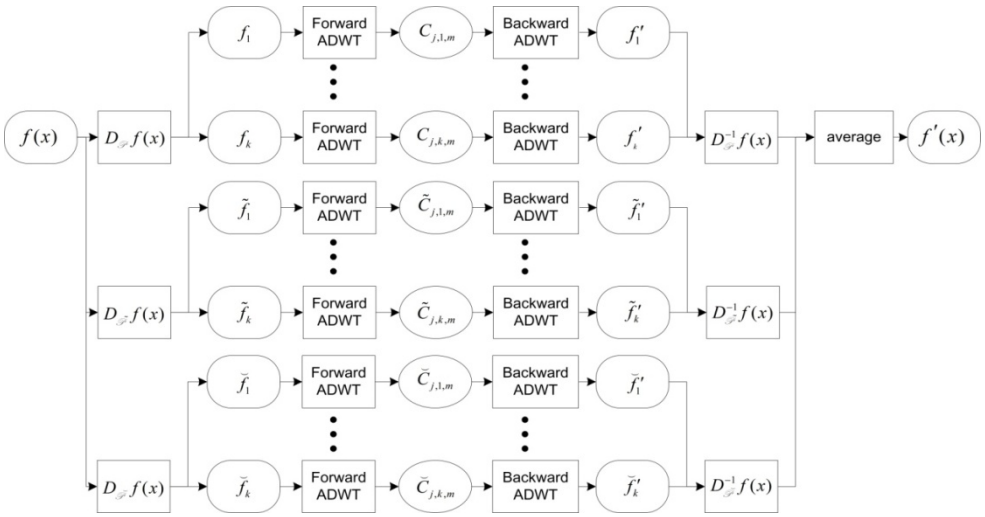

Figure 1. Steps of Forward and Backward 3D-CSST

In [14], Lim proposed the principle and the details about the construction of Compactly Supported Shearlet Transform (CSST). His work is mainly focus on 2D case. We first expand this implementation into 3D case. The steps of forward and backward 3D-CSST are given in Figure 1. The input signal $f(x)$ is first processed by shear operation in three pyramids,

represented by $\mathscr{S}$, $\tilde{\mathscr{S}}$, and $\breve{\mathscr{S}}$, which are around x, y and z axis respectively. Then the Anisotropic Discrete Wavelet Transform (ADWT) is performed on every sheared versions of input signal. The outputs of ADWT, $C_1 \cdots C_k$, $\tilde{C}_1 \cdots \tilde{C}_k$ and $\breve{C}_1 \cdots \breve{C}_k$, are the coefficients of three pyramids of the transform where the parameter k is the number of directions.

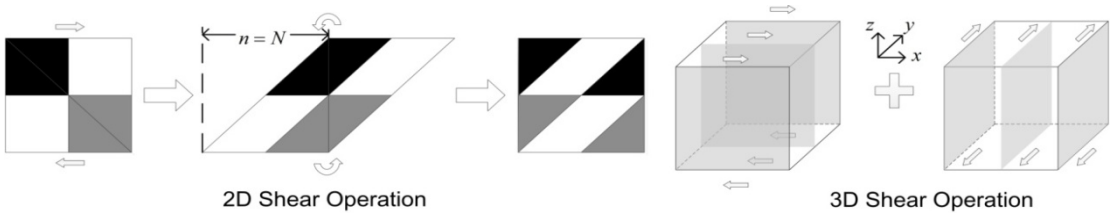

Figure 2. Shear Operation of 2D and 3D-CSST

Shear operation has an integer control parameter $n \in [-N, N]$ stands the offset that the first point of first row are shifted along one direction, where N is the size of image and minus refers to inverse direction. The illustration of shear operation with $n = N$ is given in Figure 2. With such scheme, many directions can be represented without resampling the original data. And finally, the sheared data are embedded into a rectangle with the same sizes of the original images, which guarantees no more extra memory is needed to store the sheared images. The backward shear operation just has the same steps but in an inverse order. Shear operation can be further expand into 3D case, as in Figure 2. The 2D shear operation is performed layer by layer along x-axis and then y-axis consequently.

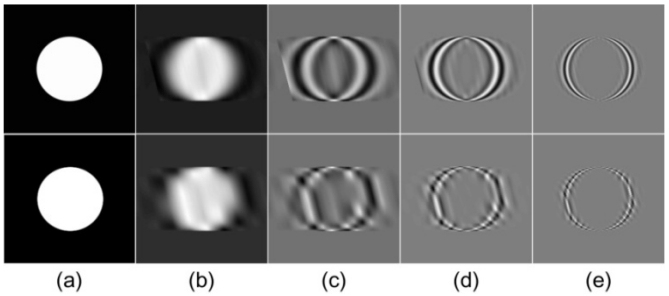

Figure 3. Reconstruction of 2D-CSST and 2D-DT-CSST
(a)The reconstructed images, (b) the reconstruction by low frequency coefficients, (c)~(e) the reconstruction by three single scale of high frequency coefficients

3D anisotropic DWT is performed next to shear operation. Anisotropic DWT is necessary, because it satisfies the definition of shearlet transform, which requires optimal representioin to curve-like singularities. In the application of image fusion, the optimal representation of curve-like singularities has little impact to the performance of fusion results. And from experiments, the value of performance indices of anisotropic DWT were indeed less than that of DWT. So the requirement of anisotropic DWT is released to common DWT. DWT has its own drawback: the shift variant property, which causes distortions in fused images. Fortunately, the shift variant property can be reduced through the structure of Dual Tree.

Using the same method in [15] which Kingsbury was using to illustrate the shift-variant of DWT and shift-invariant of dual tree complex wavelet transform (DT CWT), the comparison of reconstruction results between traditionally CSST and DT CSST were given in Figure 3. The input image was a white circle located at the center of a black background. The images in first row were the reconstruction images along one direction of DT CSST and the images in second

row were the reconstruction images along the same direction of CSST. And it should be observed from pictures in (a) that both CSST and DT CSST can reconstruct the input images precisely. But in low frequency coefficients (b) and different scales of high coefficients (c)~(e), the reconstruction images of DT CSST were much smoother than those of CSST. These differences suggested that CSST was shift-variant and DT CSST was (approximately) shift-invariant. And in 3D cases, DT structure could also effectively reduce the shift-variance of CSST.

3. Proposed Fusion Method

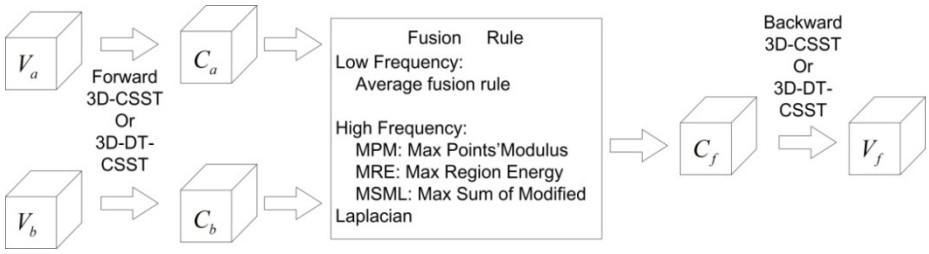

Figure 4. Steps of Proposed Medical Volume Fusion Method

The proposed fusion method in this paper belongs to the voxel-level fusion, with average rule for low frequency coefficients $C_f^l = \text{mean}(C_a^l, C_b^l)$, and three different fusion rules for high frequency coefficients:

a) Max modulus of Points' Modulus (MPM)

$$C_f = \begin{cases} C_a, |C_a| \geq |C_b| \\ C_b, |C_a| < |C_b| \end{cases} \quad (1)$$

The fused high coefficients are those have the larger modulus as in equation (1), where $C_t, t \in \{a, b, f\}$ means the high frequency coefficients, a, b label two source data respectively, f refers the fused result. This fusion rule considers only single point's information of coefficients.

b) Max Region Energy (MRE)

The fused high frequency coefficients are acquired according to (2) [12],

$$C_f = \begin{cases} C_a, |E_a| \geq |E_b| \\ C_b, |E_a| < |E_b| \end{cases} \quad (2)$$

Where $E_t = \frac{1}{N_\Omega} \sum_{p \in \Omega} \sqrt{\left(C_t(p) - \bar{C}_t\right)^2}, t \in \{a, b\}$, Ω is a local region, $\bar{C}_t$, is the mean of all C_t in Ω, N_Ω is the number of coefficients in Ω. The fused high coefficients are the coefficients that have the larger local energy. This fusion rule considers all the information of points which are in the local region Ω.

c) Max Sum of Modified Laplacian (MSML)

The fused high frequency coefficients are acquired according to (3). 3D version of Modified Laplacian index is calculated through equation (5), and the sum of them is calculated as (4), where i, j, k exhaust every point in source images and Ω is a local region around the center point (i, j, k). The parameter s equals 1 in this paper. This fusion rule also considers all the information of points which are in the local region Ω, and what's more, the center point and other points are treated differently.

$$C_f = \begin{cases} C_a, SML_a \geq SML_b \\ C_b, SML_a < SML_b \end{cases} \tag{3}$$

$$SML_t(i,j,k) = \sum_{p,q,t \in \Omega} [ML_t(i+p, j+q, k+t)]^2, t \in \{a,b\} \tag{4}$$

$$\begin{aligned} ML_t(i,j,k) = & \left|2C_t(i,j,k) - C_t(i-s,j,k) - C_t(i+s,j,k)\right| \\ & + \left|2C_t(i,j,k) - C_t(i,j-s,k) - C_t(i,j+s,k)\right|, t \in \{a,b\} \\ & + \left|2C_t(i,j,k) - C_t(i,j,k-s) - C_t(i,j,k+s)\right| \end{aligned} \tag{5}$$

The steps of proposed fusion method are given in Figure 4. Firstly, forward 3D-CSST or 3D-DT-CSST are performed to both source images, the low frequency is the average of both source coefficients, the fused high frequency fused by Equation (1~3). Finally, the backward 3D-CSST or 3D-DT-CSST are performed to fused coefficients, and the output is the fused images as represented by V_f .

4. Results and Analysis

In this section, the performances of proposed methods were evaluated on 4 human brain subjects, and compared with 2D, 3D-DWT [4] and 2D, 3D-DTCWT [5] based methods. The human study was approved by our Institutional Review Board. MR examinations were performed with a 3.0T MR system (Signa HDxt, GE, USA), using an 8-channel head coil. A 3D T2* weighted multi echo gradient echo sequence was used with the following parameters: FA=20°; TR=57ms; number of TEs=8; first TE=5.7ms; uniform TE spacing (ΔTE)=6.7ms; BW=±41.67 kHz; field of view (FOV)=24cm; a range of resolutions were tested: 0.57×0.75×2 mm^3. The 3D T2* magnitude and QSM images, which are reconstructed by the tools of [16], are interpolated to $128 \times 128 \times 128$. In QSM processing, the magnetic fields outside the brain parenchyma were corrupted by noise, therefore, QSM regions were cropped by masks, which were obtained by brain extraction tool (BET) of [17]. Consequently, the experiments were evaluated by the valid data in all masks.

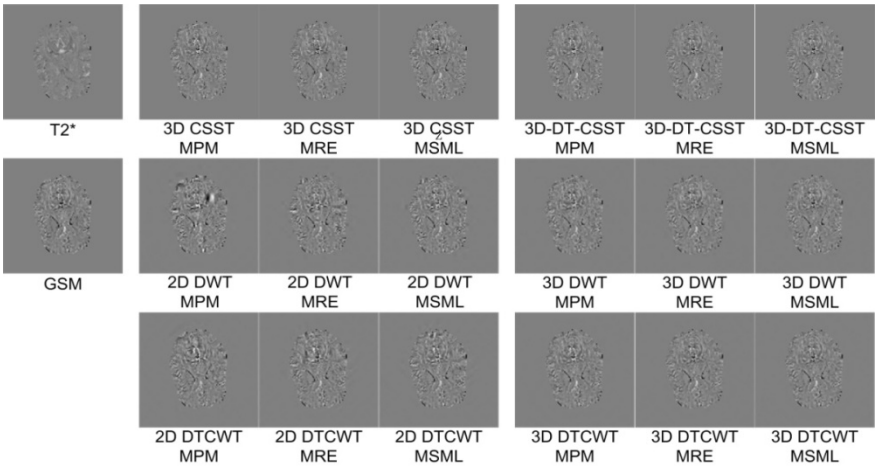

Figure 5. Inter Frame Differences for 2D and 3D Fusion Methods

Firstly, we evaluated the consistency in the third dimension between 2D methods and 3D methods. 2D methods fused source images layer by layer, 3D methods directly fused all 3D images as a whole. Consistency along the third axis can be evaluated by both the perspective impression of inter frame difference (IFD) images, as shown in Figure 5, and their mutual

information (IFD_MI) [18, 19]. From Figure 5, it can be noticed that the fused images by 2D methods have several obvious distortions which resembles to neither of the source images. While in the results by 3D methods, the IDF images of were much consistent to the IDF of source data, suggested that the IDF images were highly correlated to the IDF of source images. The difference among the 3D methods can hardly be noticed. This conclusion can be comfirmed by IFD_MI, as listed in Table 1. Only the first subjects are listed for the limitation of the paper. In this experiment, only the voxels in the common region of two masks were calculated by equation (6). Suppose conventional IFD_MI without mask is represented by $MI_i(D_a^i, D_b^i, D_f^i)$, where D_a^i, D_b^i, D_f^i are the inter frame difference images for both sources V_a^i, V_b^i and V_f^i fused images, $D_t^i = V_t^{i+1} - V_t^i, t \in \{a, b, f\}$, *i* represents that the current layer is the *i*-th layer, *N* refers to the whole number of layers along the third axis, and $\bullet$ refers to point-wise multiplication. The quality indices of The method of 3D-DT-CSST with MSML rule has the highest value of IFD_MI, and all the values for 3D methods are higher than the 2D methods with same rule.

$$\text{IDF\_MI} = \frac{1}{N-1}\sum_{i=1}^{N-1}\left(MI_i(D_a^i, D_b^i, D_f^i) \bullet (Mask^{i+1} \cup Mask^i)\right) \quad (6)$$

Table 1. IFD_MI for the First Subject

IFD_MI	2D DWT	2D DTCWT	3D DWT	3D DTCWT	3D CSST	3D DT CSST
MPM	1.8443	1.7659	1.8905	2.2147	2.0943	2.5409
MRE	1.7349	1.7650	1.8989	2.1558	2.0257	2.3809
MSML	1.7274	1.7503	2.0965	2.3432	2.0374	2.5899

One layer of each coronal, axial and sagittal images are selected as the representations, the source and result images are shown in Figure 6 to Figure 8. From the perspective impression, it was hard to tell which fusion method was better, because the result images were much similar to each other. The distinctions among them can be noticed only after carefully observation. This phenomenon suggested that both the proposed methods and all conventional methods could fulfill the task. Two performance indices, Mutual Information (MI) and $Q^{AB|F}$ [20], were selected to evaluate the proposed methods, and were expanded into 3D version. They were listed in Table 2. It should be noticed that the quality indices of proposed methods were larger than the methods that based on DWT or DT CWT. And in the case of 3D-CSST and 3D-DT-CSST, the rule of MSML had the highest indices. The same phenomena could also be noticed in other subjects which were omitted for the limitation of the paper.

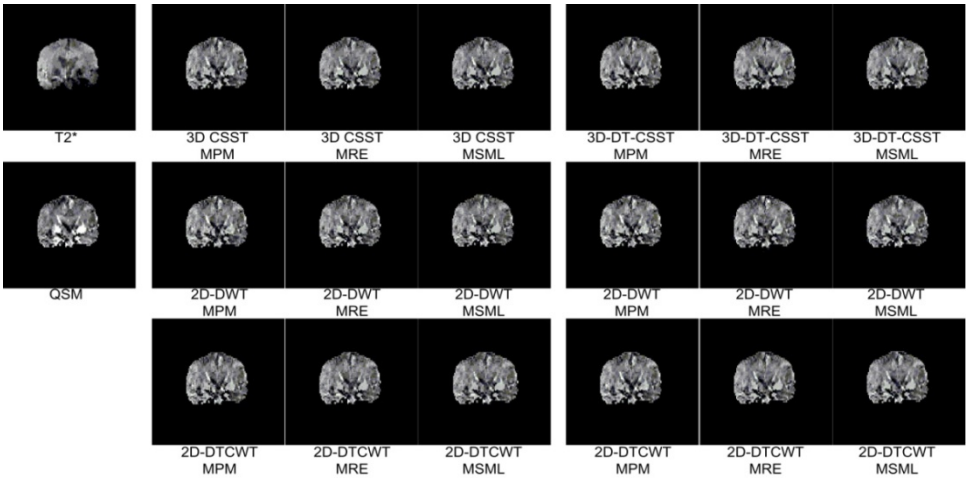

Figure 6. Coronal Source and Result Images

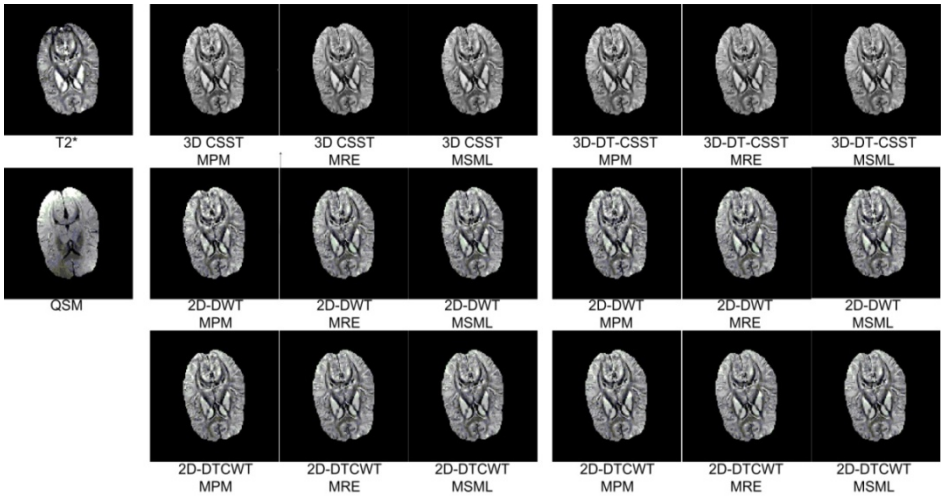

Figure 7. Axial Source and Result Images

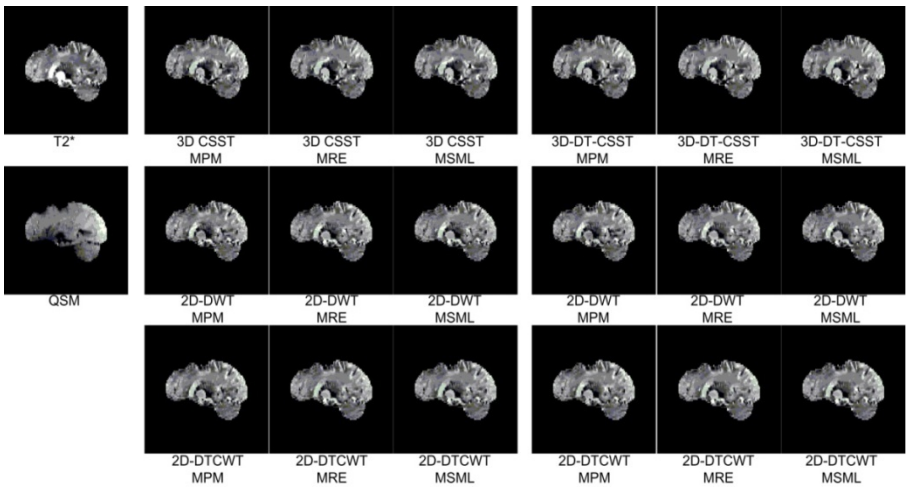

Figure 8. Sagittal Source and Result Images

Table 2. Performance of the First Subject

First subject		2D DWT	2D DTCWT	3D DWT	3D DTCWT	3D CSST	3D DT CSST
MPM	MI	1.1652	1.2168	1.1615	1.2404	1.2574	1.2718
	$Q^{AB|F}$	0.1824	0.1985	0.1820	0.2109	0.2182	0.2264
MRE	MI	1.1596	1.2323	1.1471	1.2561	1.3054	1.3112
	$Q^{AB|F}$	0.1987	0.2185	0.1975	0.2351	0.2442	0.2568
MSML	MI	1.1566	1.2339	1.2043	1.2617	1.3062	**1.3132**
	$Q^{AB|F}$	0.1977	0.2158	0.2257	0.2402	0.2534	**0.2656**

5. Conclusion

Conventional 2D image fusion method can only fuse the 3D MRI images layer by layer, which leads to the loss of inter layer correlation of 3D images. In this paper, the 3D medical image fusion methods based on 3D-CSST and its shift invariant version, 3D-DT-CSST, were proposed. From the principles of methods and the experiments the following conclusions can be drawn: 1) the 3D-transform based methods had a better consistency along the third axis than conventional 2D-transform based methods. 2) From both perspective impression and the performance indices, the proposed medical fusion methods were better than 3D-DWT or 3D-DTCWT. 3) Among the fusion rules of 3D-CSST or 3D-DT-CSST based methods, the MSML rule had a better performance than other two rules.

Acknowledgements

This work was supported in part by the National Nature Science Foundation of China (No.611390003). The authors also would like to thank Dr. Yi Wang for data providing and Dr. Tim Vartanian, Dr. Jai Perumal, and Dr. Nancy Nealon for data collection, as well as to those reviewers and editors for their dedicated works.

References

[1] CR Hatt, AK Jain, V Parthasarathy, A Lang, AN Raval. MRI-3D ultrasound-X-ray image fusion with electromagnetic tracking for transendocardial therapeutic injections: In-vitro validation and in-vivo feasibility. *Computerized Medical Imaging and Graphics*. 2013; 37(2): 162-173.
[2] D Clevert, A Helck, PM Paprottka, P Zengel, C Trumm, MF Reiser. Ultrasound-guided image fusion with computed tomography and magnetic resonance imaging. Clinical utility for imaging and interventional diagnostics of hepatic lesions. *Der Radiologe*. 2012; 52(1): 63-69.
[3] G Lei, HH Li, YS Bao. Image fusion. Beijing: publishing house of electronics industry. 2008: 80-81.
[4] G Pajares, J Manuel de la Cruz. A wavelet-based image fusion tutorial. *Pattern Recognition*. 2004: 37(9): 1855-1872.
[5] Y Zou, X Liang, T Wang. Visible and Infrared Image Fusion Using the Lifting Wavelet. *TELKOMNIKA Indonesian Journal of Electrical Engineering*. 2013; 11(11): 6290-6295.
[6] PR Hill, DR Bull, CN Canagarajah. Image fusion using a new framework for complex wavelet transforms. *IEEE International Conference on Image Processing.* Genoa. 2005; 2: II-1338-41.
[7] H Lu, L Zhang, S Serikawa. Maximum local energy: An effective approach for multisensor image fusion in beyond wavelet transform domain. *Computers & Mathematics with Applications.* 2012; 64(5): 996-1003.
[8] L Wang, B Li, L Tian, EGGDD: An explicit dependency model for multi-modal medical image fusion in shift-invariant shearlet transform domain. *Information Fusion*. 2013.
[9] GR Easley, D Labate, F Colonna. Shearlet-based total variation diffusion for denoising. *IEEE Trans Image Process*. 2009; 18(2): 260-268.
[10] S Yi, D Labate, GR Easley. A shearlet approach to edge analysis and detection. *IEEE Trans Image Process*. 2009; 18(5): 929-941.
[11] PS Negi, D Labate. 3-D discrete shearlet transform and video processing. *IEEE Trans Image Process.* 2012; 21(6): 2944-2954.
[12] P Feng, J Wang, B Wei. A Fusion Algorithm for GFP Image and Phase Contrast Image of Arabidopsis Cell Based on SFL-Contourlet Transform. *Computational and mathematical methods in medicine.* 2013.
[13] J Liu, J Yang, B Li. Multi-focus Image Fusion by SML in the Shearlet Subbands. *TELKOMNIKA Indonesian Journal of Electrical Engineering*. 2014; 12(1): 618-626.
[14] WQ Lim. The discrete shearlet transform: a new directional transform and compactly supported shearlet frames. *IEEE Trans Image Process*. 2010; 19(5): 1166-1180.
[15] N Kingsbury. Complex wavelets for shift invariant analysis and filtering of signals. *Applied and computational harmonic analysis*. 2001; 10(3): 234-253.
[16] T Liu, C Wisnieff, M lou. Nonlinear formulation of the magnetic field to source relationship for robust quantitative susceptibility mapping. *Magn Reson Med*. 2013; 69(2): 467-476.
[17] SM Smith. Fast robust automated brain extraction. *Human brain mapping*. 2002; 17(3): 143-155.
[18] Q Zhang, Y Chen, L Wang. Multisensor video fusion based on spatial-temporal salience detection. *Signal Processing*. 2013; 93(9): 2485-2499.
[19] Q Zhang, L Wang, Z Ma. A novel video fusion framework using surfacelet transform. *Optics Communications*. 2012; 285(13): 3032-3041.
[20] V Petrovi, C Xydeas. *On the effects of sensor noise in pixel-level image fusion performance*. FUSION 2000. Proceedings of the Third International Conference. Paris. 2000; 2: WEC3/14-WEC3/19.